Supplementary Information

Visible-Light NO-Photolysis of Ruthenium Nitrosyl Complexes with N2O2 Ligands Bearing π-Extended Rings and their Photorelease Dynamics

Minyoung Kim, Seongchul Park, Dayoon Song,

Dohyun Moon, Youngmin You, Manho Lim, and Hong-In Lee

< Table of Contents >

Fig. S1. IR spectra of (A) Ru(salophen)(NO)Cl (**1**), (B) photoproduct of **1**, (C) Ru(naphophen)(NO)Cl (**2**), and (D) photoproduct of **2**.

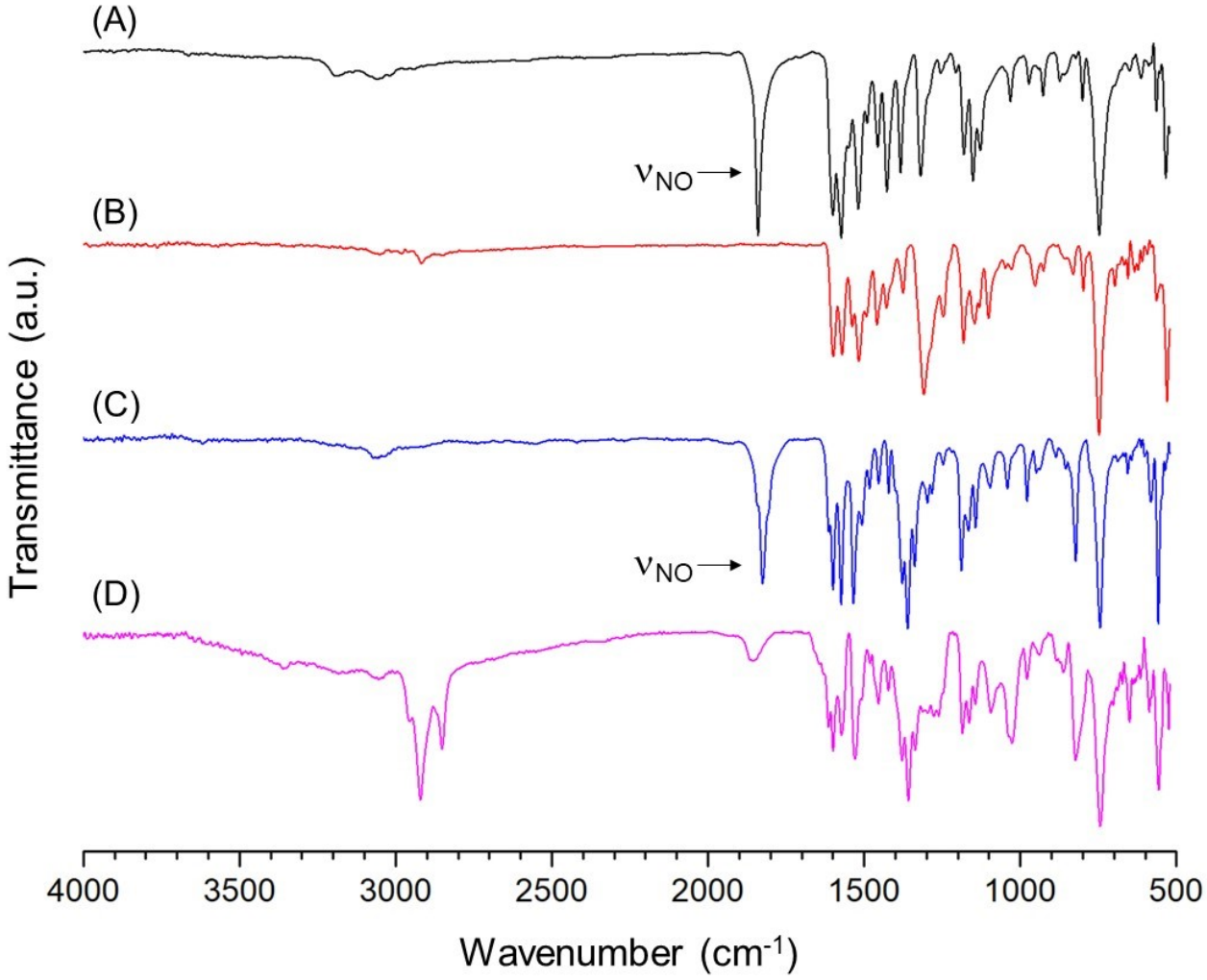

Fig. S2. ORTEP diagram of Ru(naphophen)(ON)Cl (**2LI**), a linkage isomer of Ru(naphophen)(NO)Cl (**2**), with 33% probability ellipsoids and atom numbering scheme. Hydrogen atoms are omitted for clarity. The ORTEP diagram shows **2LI** portion out of **2LI**·CH_3CN crystal

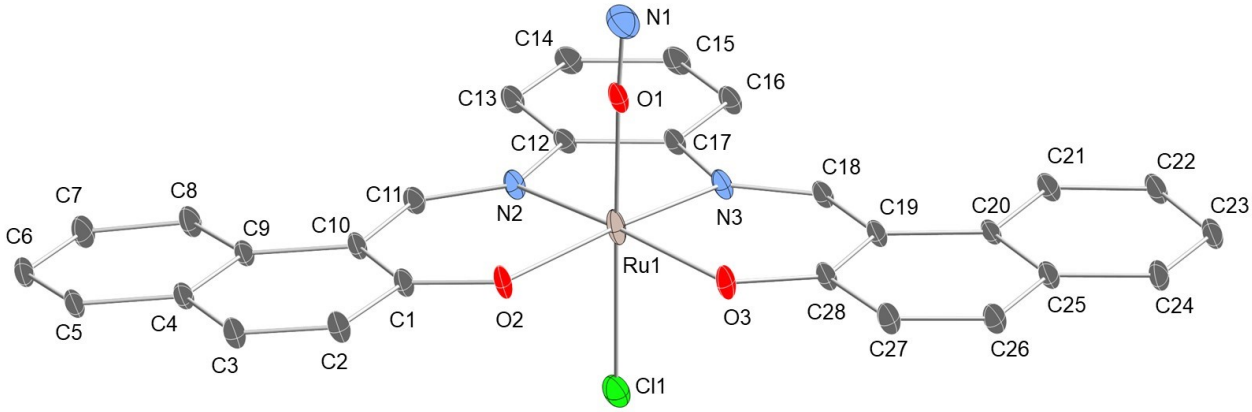

Fig. S3. UV/Vis absorption spectra of (A) Ru(salophen)(NO)Cl (**1**) and (B) Ru(naphophen)(NO)Cl (**2**) in acetonitrile under dark condition. $[\mathbf{1}]_0 = 4.3 \times 10^{-5}$ M and $[\mathbf{2}]_0 = 6.1 \times 10^{-5}$ M. (Blue = 0 day, Black = 1, 2, 5 days, Red = 7days)

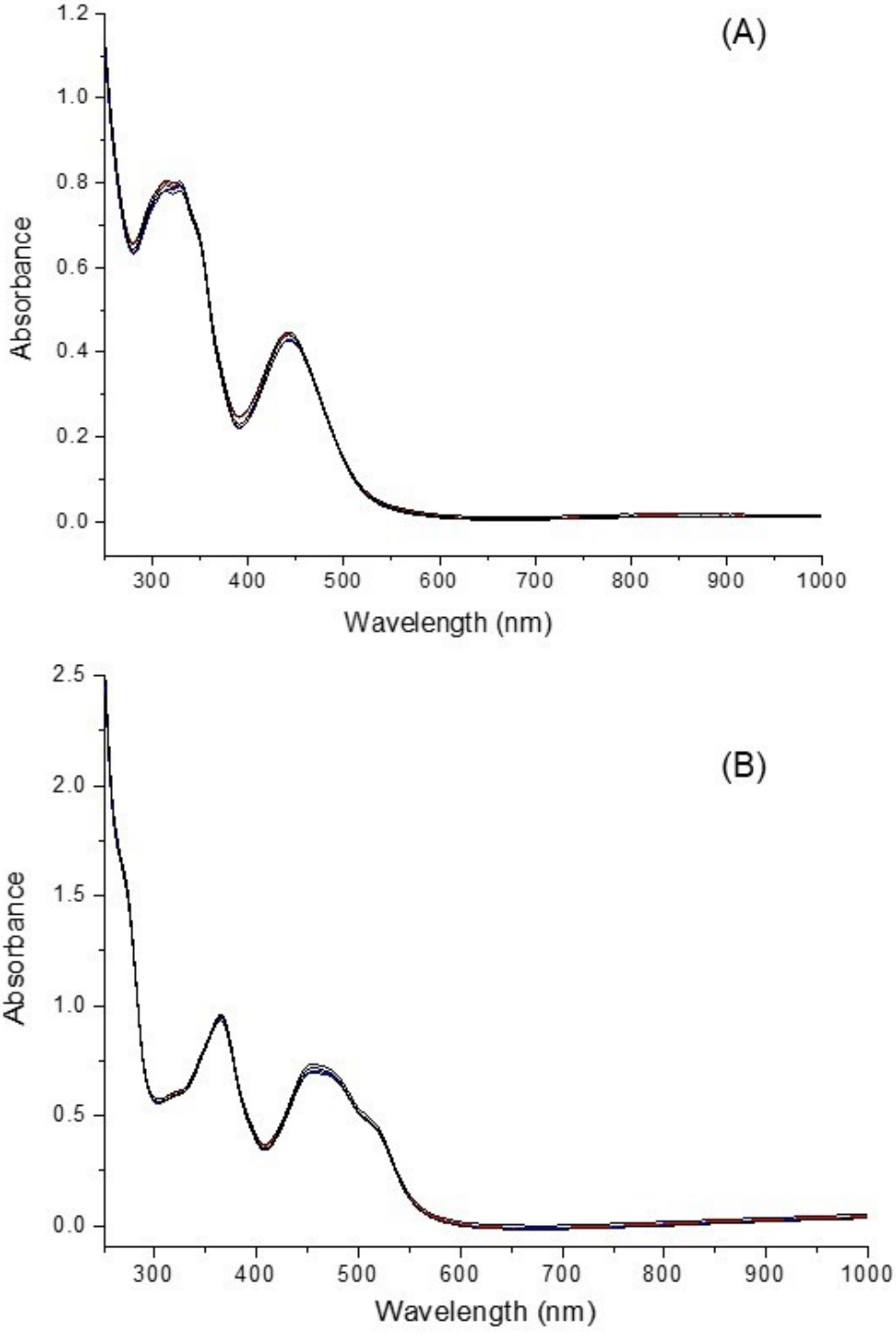

Fig. S4. (A) UV/Vis absorption spectral change of 100 μM Ru(salophen)(NO)Cl (**1**) dissolved in CH_3CN in a quartz cell (beam path length = 1 cm) recorded during continuous photoirradiation (λ_{ex} = 459 nm, photon flux = 3.83×10^{-9} einstein s^{-1}) for 9 min. (B) Plot of the product concentration for the photolysis reaction of **1** as a function of input photons. The red line corresponds to the linear fit of the data. PCQY refers to the photochemical quantum yield determined using eq. 2.

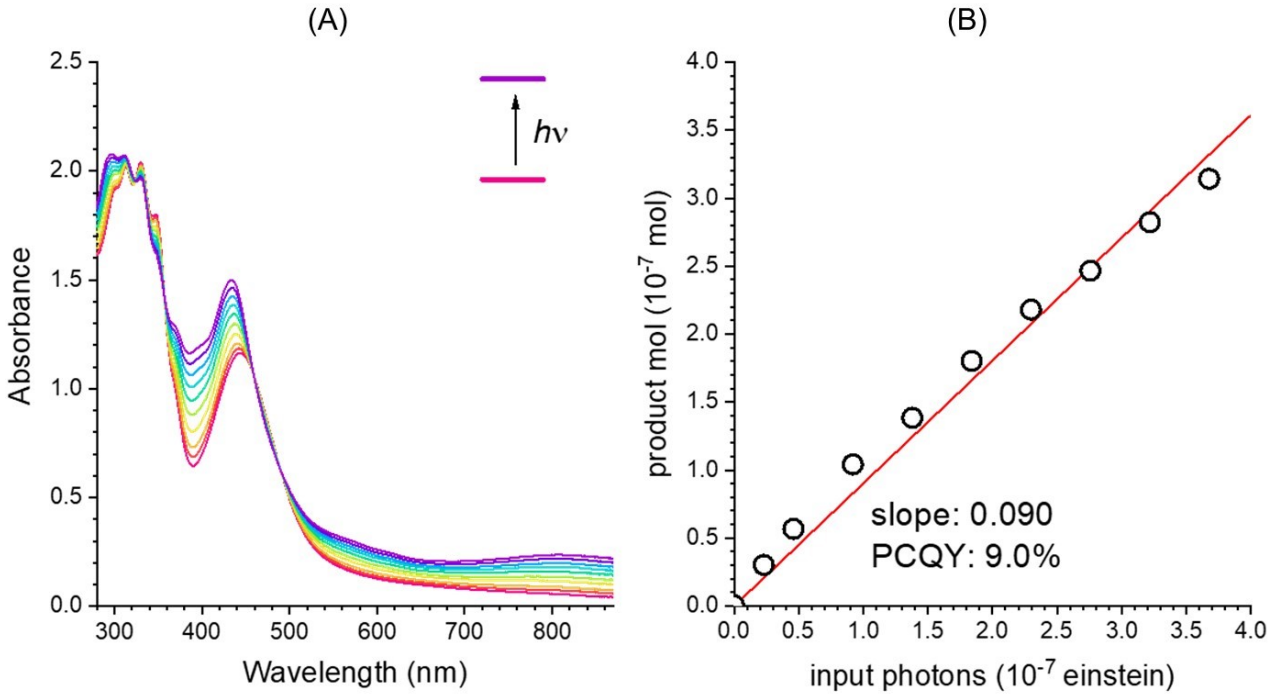

Fig. S5. (A) UV/Vis absorption spectral change of 100 μM Ru(naphophen)(NO)Cl (**2**) dissolved in CH_3CN in a quartz cell (beam path length = 1 cm) recorded during continuous photoirradiation (λ_{ex} = 489 nm, photon flux = 3.83 × 10^{-9} einstein s^{-1}) for 9 min. (B) Plot of the product concentration for the photolysis reaction of **2** as a function of input photons. The red line corresponds to the linear fit of the data. PCQY refers to the photochemical quantum yield determined using eq. 2.

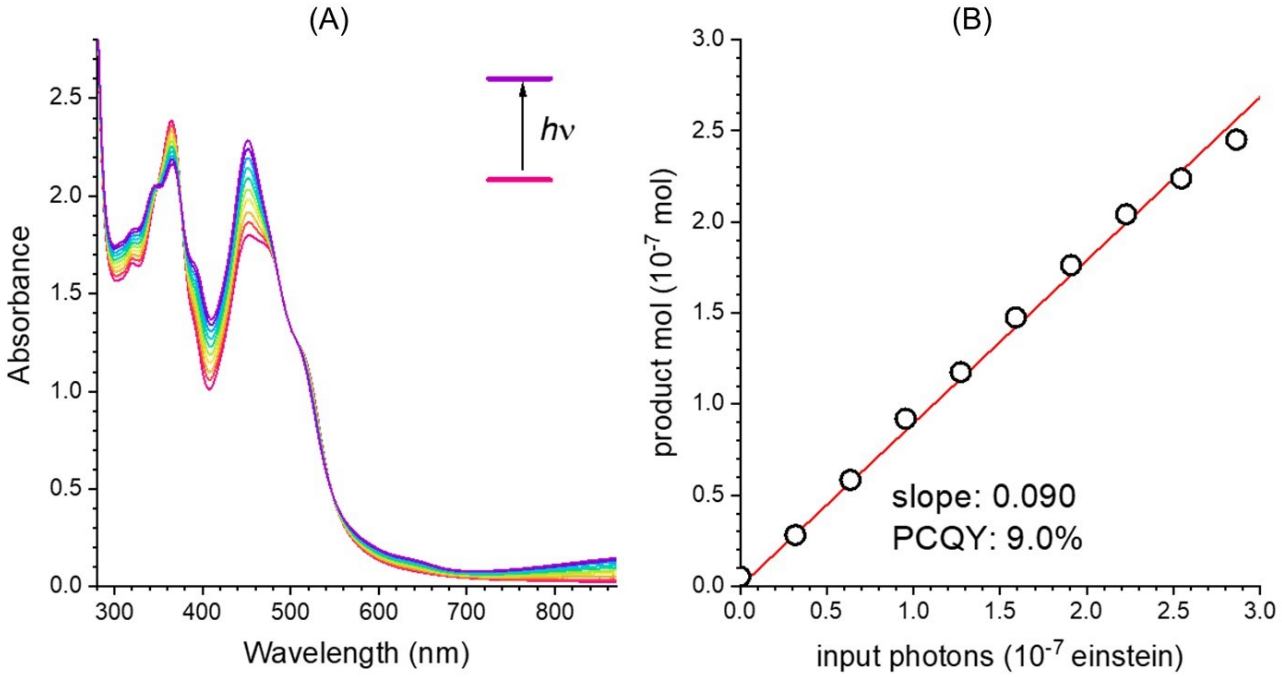

Fig. S6. EPR spectra obtained from the frozen solutions of (A) **1** and (B) **2** in CH_3CN after exposed to room light for 9 hrs, and their corresponding numerical simulations. EPR experimental conditions are same as in fig. 4. Simulation parameters for (A) are microwave frequency = 9.421 GHz, ***g*** = [2.30 2.12 1.84], and linewidth = 50 G and for (B) microwave frequency = 9.409 GHz, ***g*** = [2.29 2.08 1.88], and linewidth = 70 G.

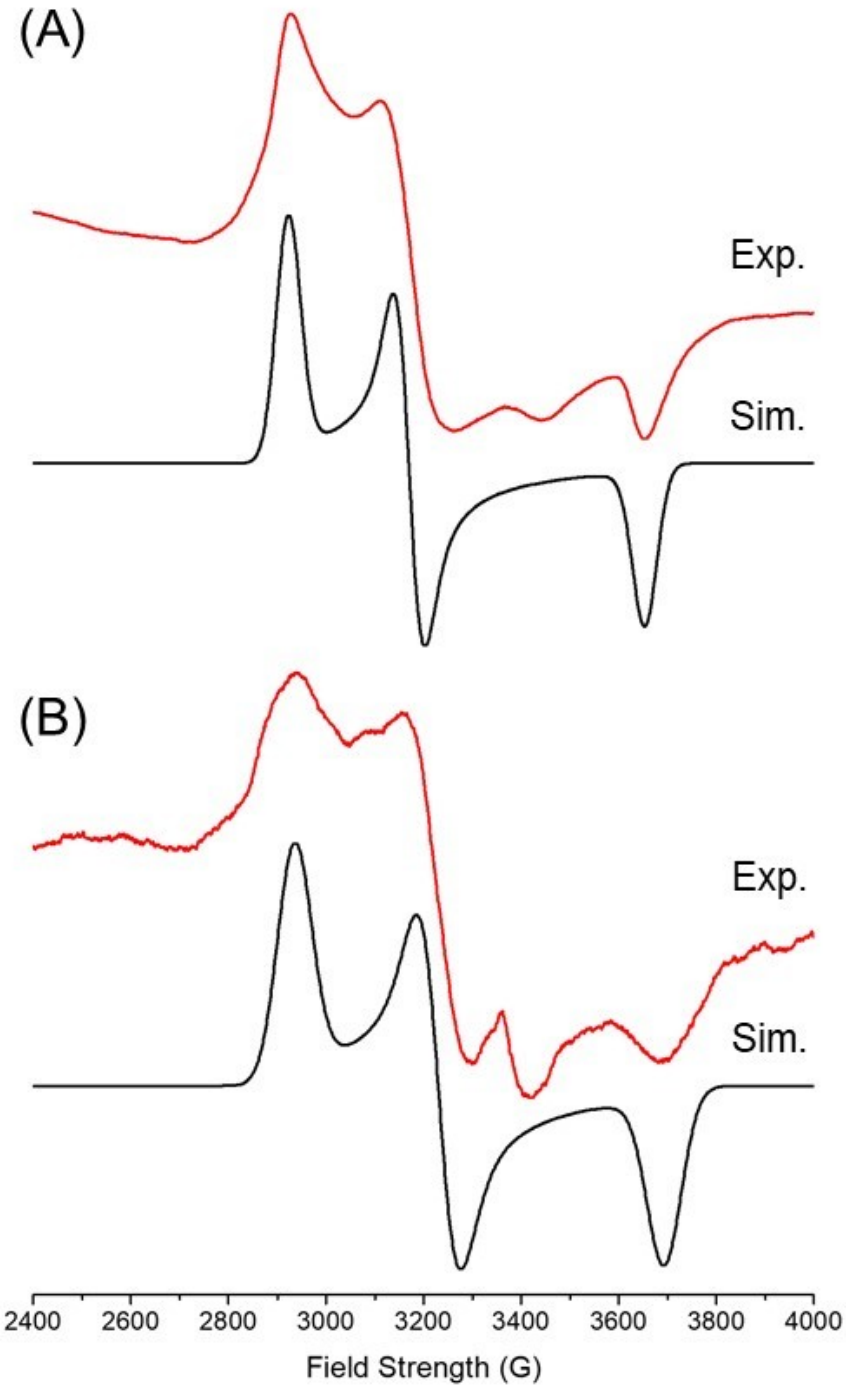

Fig. S7. 500 MHz ^{1}H NMR spectra of Ru(salophen)(NO)Cl (**1**) dissolved in d_6-DMSO at 18, 7, 4, and 0 days after exposed to room light, respectively. For observing the photoreaction of **1**, the NMR tube containing **1** was left on a bench table for a certain time and then delivered to a spectrometer.

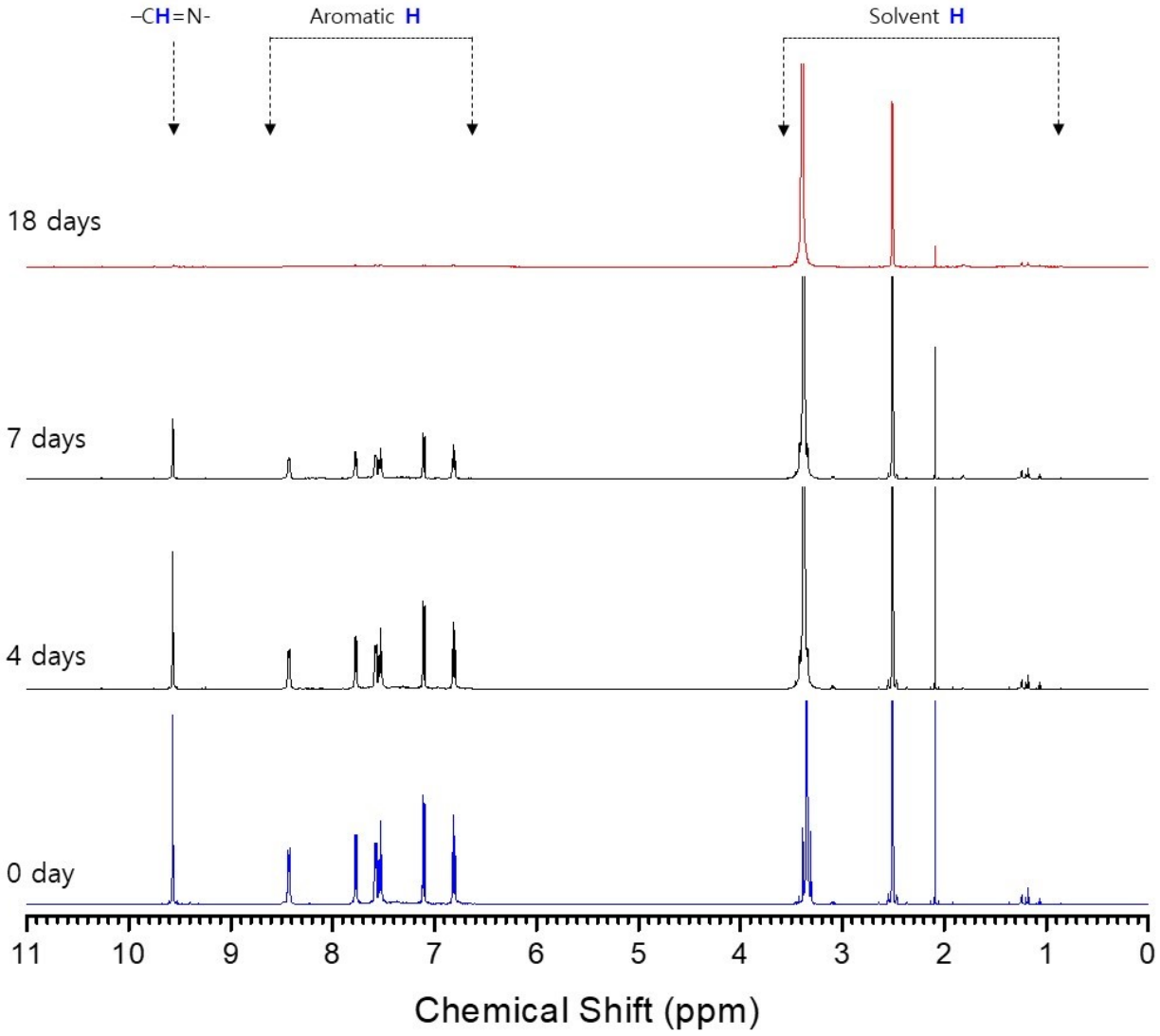

Fig. S8. 500 MHz ^{1}H NMR spectra of Ru(naphophen)(NO)Cl (**2**) dissolved in d_6-DMSO at 17, 5, 3, and 0 days after being exposed to room light, respectively. For observing the photoreaction of **2**, the NMR tube containing the solution of **2** was left on a bench table for a certain time and then delivered to a spectrometer.

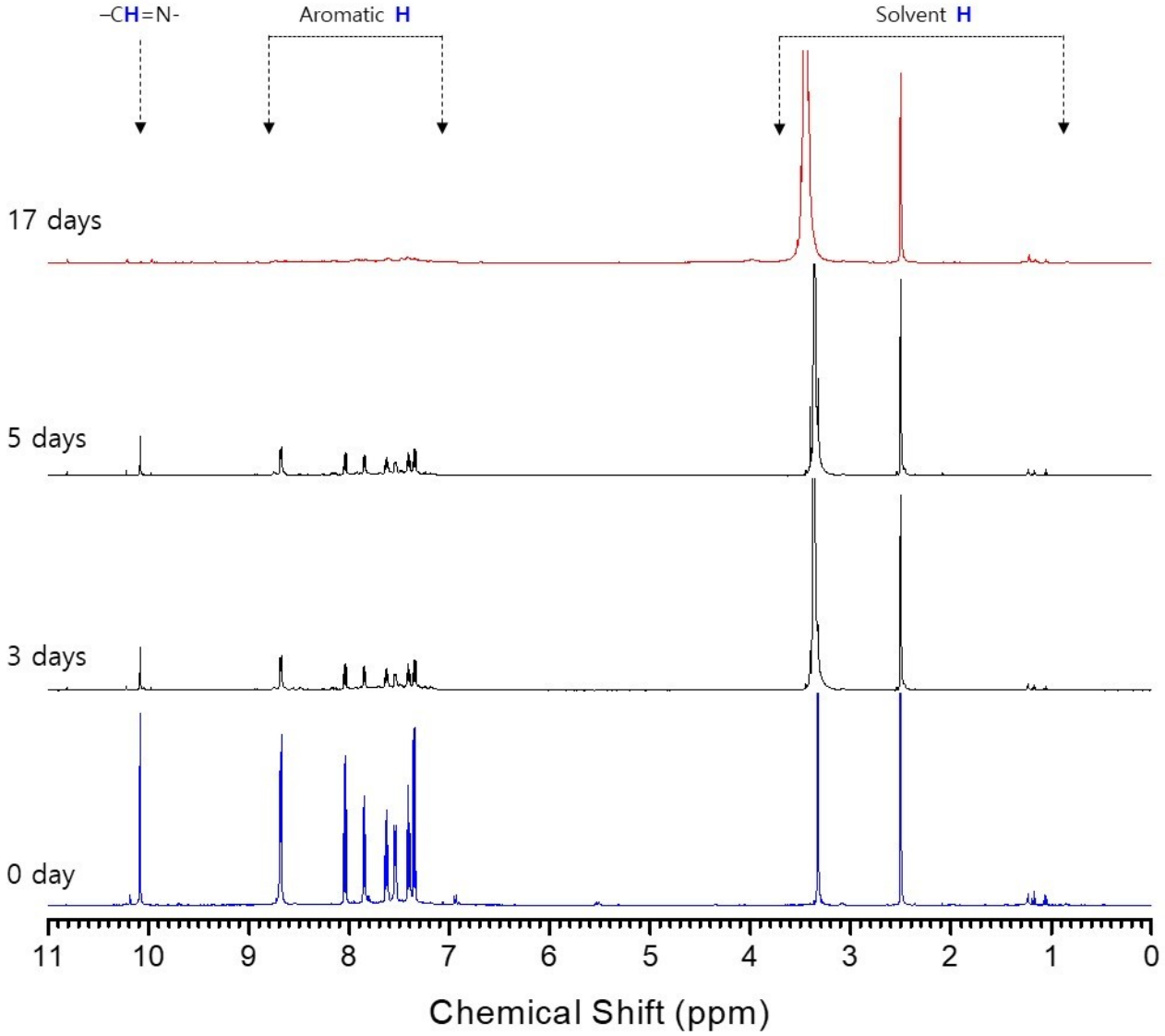

Fig. S9. The shapes of the selected MOs of Ru(salophen)(NO)Cl (**1**). MOs, which are related to the configuration interactions in table 1, are graphically represented.

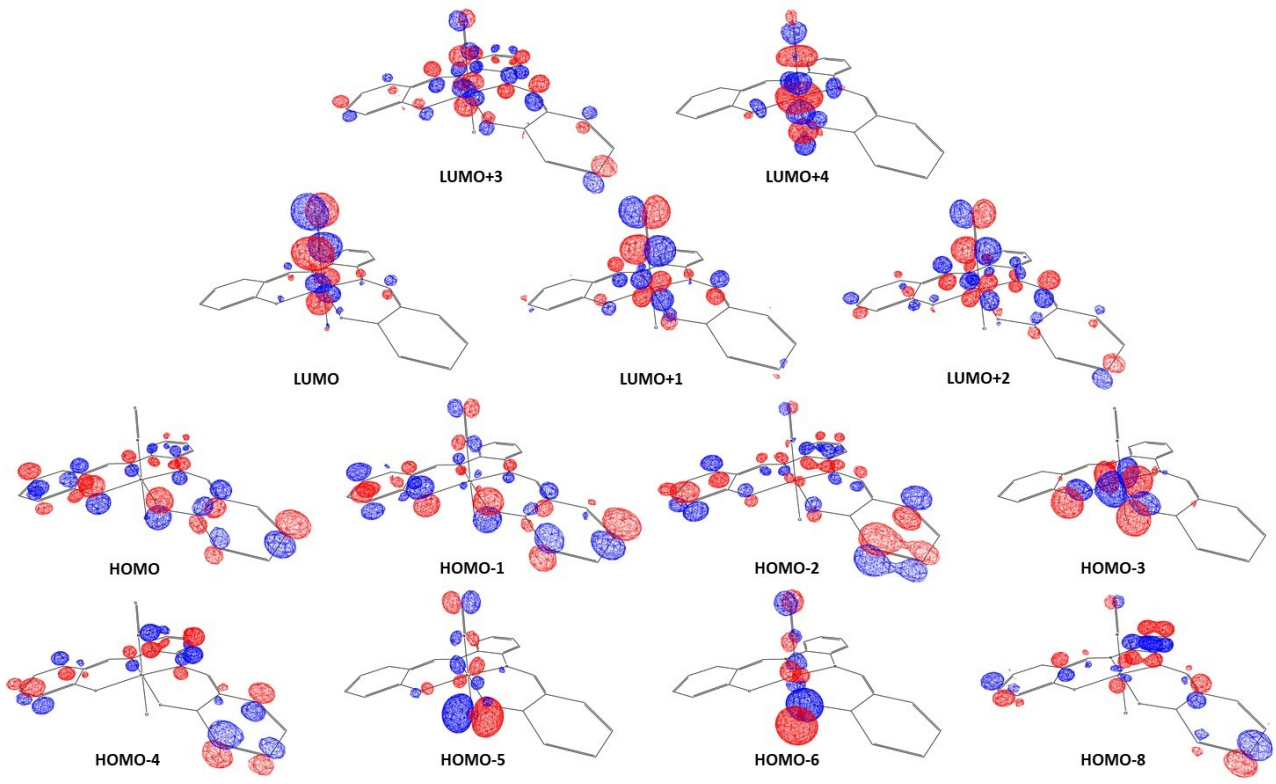

Fig. S10. The shapes of the selected MOs of Ru(naphophen)(NO)Cl (**2**). MOs, which are related to the configuration interactions in table 2, are graphically represented.

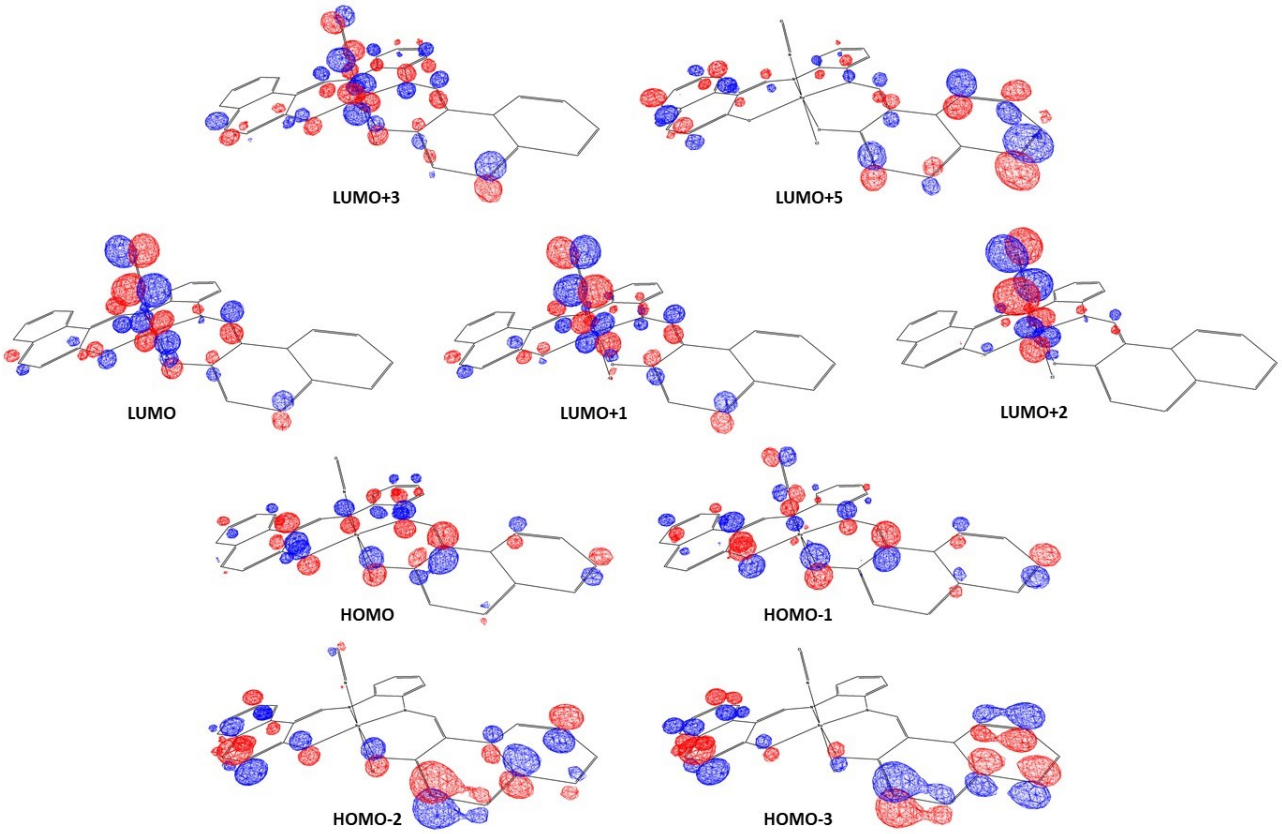

Table S1. Crystal data and structure refinements for (A) [Ru(salophen)(NO)Cl]CH_3CN (**1**·CH_3CN) (B) [Ru(salophen)(CH_3OH)Cl]CH_3OH (**1′**·CH_3OH), and (C) Ru(naphophen)(CH_3CN)Cl (**2′**)

	(A)	(B)	(C)
CCDC numbers	2107047	2106758	2107296
Compounds	**1**·CH_3CN	**1′**·CH_3OH	**2′**
Empirical formula	$C_{22}H_{17}ClN_4O_3Ru$	$C_{22}H_{22}ClN_2O_4Ru$	$C_{30}H_{21}ClN_3O_2Ru$
Formula weight	521.91	514.93	592.02
Temperature, K	173(2)	173(2)	173(2)
Wavelength, Å	0.80000	0.63000	0.70000
Crystal system	Monoclinic	Triclinic	Orthorhombic
Space group	$P2_1/c$	$P\bar{1}$	P*ccn*
a, Å	9.4410(19)	7.4300(15)	21.409(4)
b, Å	17.008(3)	11.531(2)	32.303(7)
c, Å	13.085(3)	13.619(3)	7.3530(15)
α, °	90	109.75(3)	90
β, °	100.91(3)	102.83(3)	90
γ, °	90	102.50(3)	90
Volume, Å^3	2063.1(7)	1015.3(4)	5085.2(18)
Z	4	2	8
Reflection collected	14876	11145	30793
Independent Reflections	4195 (R_{int}= 0.0904)	5657 (R_{int} = 0.0259)	5090 (R_{int} = 0.0335)
Goodness-of-fit on F^2	1.117	1.102	1.126
Final R indices $[I > 2\sigma(I)]$[a,b]	R_1 = 0.0632, wR_2 = 0.1790	R_1 = 0.0340, wR_2 = 0.0952	R_1 = 0.0362, wR_2 = 0.1053
R indices (all data)	R_1 = 0.0780, wR_2 = 0.1898	R_1 = 0.0364, wR_2 = 0.0966	R_1 = 0.0419, wR_2 = 0.1093
Largest diff. peak and hole, e·Å^{-3}	1.548 and -1.940	0.825 and -1.394	0.550 and -1.222

[a] $R_1 = \Sigma||F_0|-|F_c||/\Sigma|F_0|$, [b] $wR_2 = [\Sigma w(F_0^2-F_c^2)^2/\Sigma wF_0^4]^{1/2}$

Table S2. Selected bond lengths and angles for (A) [Ru(salophen)(NO)Cl]CH_3CN (**1**·CH_3CN) (B) [Ru(salophen)(CH_3OH)Cl]CH_3OH (**1′**·CH_3OH), and (C) Ru(naphophen)(CH_3CN)Cl (**2′**)

(A) **1**·CH_3CN		(B) **1′**·CH_3OH		(D) **2′**	
Bond lengths (Å)					
N1-O1	1.150(6)				
Ru1-N1	1.744(5)	Ru1-O3	2.0692(15)	Ru1-N3	2.058(3)
Ru1-N2	2.031(4)	Ru1-N2	1.992(2)	Ru1-N1	1.975(2)
Ru1-N3	2.028(4)	Ru1-N1	1.9776(19)	Ru1-N2	1.983(2)
Ru1-O2	2.037(4)	Ru1-O2	2.0237(16)	Ru1-O1	2.025(2)
Ru1-O3	2.034(4)	Ru1-O1	2.0119(18)	Ru1-O2	2.016(2)
Ru1-Cl1	2.3547(15)	Ru1-Cl1	2.3305(8)	Ru1-Cl1	2.3377(9)
Bond angles (°)					
Ru1-N1-O1	174.7(4)				
N1-Ru1-Cl1	177.14(15)	O3-Ru1-Cl1	178.11(4)	N3-Ru1-Cl	176.08(7)
N2-Ru1-O3	172.59(15)	N2-Ru1-O1	178.04(6)	N1-Ru1-O2	176.46(9)
N3-Ru1-O2	173.79(15)	N1-Ru1-O2	176.28(6)	N2-Ru1-O1	176.28(9)
N1-Ru1-N2	95.41(19)	O3-Ru1-N2	93.47(7)	N3-Ru1-N1	89.47(10)
N1-Ru1-N3	93.44(18)	O3-Ru1- N1	88.50(7)	N3-Ru1-N2	92.02(10)
N1-Ru1-O2	91.90(18)	O3-Ru1-O2	89.39(7)	N3-Ru1-O1	86.42(9)
N1-Ru1-O3	91.28(18)	O3-Ru1-O1	85.39(7)	N3-Ru1-O2	90.49(9)
N2-Ru1-N3	81.72(18)	N2-Ru1-N1	82.98(8)	N1-Ru1-N2	84.07(10)
N2-Ru1-O2	94.63(17)	N2-Ru1-O2	94.09(7)	N1-Ru1-O1	92.54(9)
N2-Ru1-Cl1	87.32(12)	N2-Ru1-Cl1	88.32(6)	N1-Ru1-Cl1	90.10(7)
N3-Ru1-O3	94.71(17)	N1-Ru1-O1	95.39(7)	N2-Ru1-O2	92.39(9)
N3-Ru1-Cl1	87.77(12)	N1-Ru1-Cl1	91.10(5)	N2-Ru1-Cl1	91.81(7)
O2-Ru1-O3	88.33(16)	O2-Ru1-O1	87.49(7)	O1-Ru1-O2	90.99(8)
O2-Ru1-Cl1	87.05(11)	O2-Ru1-Cl1	91.10(5)	O1-Ru1-Cl1	89.71(6)
O3-Ru1-Cl1	86.04(11)	O1-Ru1-Cl1	92.81(5)	O2-Ru1-Cl1	90.18(6)

Table S3. Crystal data and structure refinements for [Ru(naphophen)(ON)Cl]CH_3CN (**2LI**·CH_3CN)

CCDC number	2107785
Compound	**2LI**·CH_3CN
Empirical formula	$C_{30}H_{21}ClN_4O_3Ru$
Formula weight	622.03
Temperature, K	173(2)
Wavelength, Å	0.63000
Crystal system	Triclinic
Space group	$P\bar{1}$
a, Å	10.532(2)
b, Å	11.190(2)
c, Å	12.057(2)
α, °	94.94(3)
β, °	113.97(3)
γ, °	98.24(3)
Volume, Å^3	1268.5(5)
Z	2
Reflection collected	11849
Independent	6856
Reflections	(R_{int} = 0.0205)
Goodness-of-fit on F^2	1.068
Final R indices	R_1 = 0.0496,
$[I > 2\sigma(I)]$[a,b]	wR_2 = 0.1244
R indices	R_1 = 0.0539,
(all data)	wR_2 = 0.1268
Largest diff. peak and hole, e·Å^{-3}	3.202 and -1.917

[a]$R_1 = \Sigma||F_0|-|F_c||/\Sigma|F_0|$, [b]$wR_2 = [\Sigma w(F_0^2-F_c^2)^2/\Sigma wF_0^4]^{1/2}$

Table S4. Selected bond lengths and angles for [Ru(naphophen)(ON)Cl]CH_3CN (**2LI**·CH_3CN)

Bond lengths (Å)	
O1-N1	1.072(4)
Ru1-O1	1.854(2)
Ru1-N2	2.005(2)
Ru1-N3	2.007(3)
Ru1-O2	2.027(2)
Ru1-O3	2.0328(19)
Ru1-Cl1	2.3157(11)
Bond angles (°)	
Ru1-O1-N1	177.1(4)
O1-Ru1-Cl1	178.13(6)
N2-Ru1-O3	173.27(10)
N3-Ru1-O2	173.34(10)
O1-Ru1-N2	94.57(10)
O1-Ru1-N3	92.76(10)
O1-Ru1-O2	93.14(10)
O1-Ru1-O3	91.35(10)
N2-Ru1-N3	83.33(10)
N2-Ru1-O2	93.12(10)
N2-Ru1-Cl1	87.24(8)
N3-Ru1-O3	93.22(9)
N3-Ru1-Cl1	87.92(9)
O2-Ru1-O3	89.73(8)
O2-Ru1-Cl1	86.29(8)
O3-Ru1-Cl1	86.87(8)

Photoexcitation Dynamics of Ru(salophen)(NO)Cl (1)

The photodissociation dynamics of NO from Ru(salophen)(NO)Cl (**1**) in DMSO were investigated over broad time range from 0.3 ps to 1 μs after excitation at 320 nm using a femtosecond time-resolved infrared (TRIR) spectroscopy. In femtosecond TRIR spectroscopy, an equilibrium sample was excited by an intense femtosecond laser pulse (1.5 – 3 μJ, 120 fs, 320 nm pulse in this experiment), and another femtosecond mid-IR pulse was used to measure a series of transient vibrational spectra of the photoexcited sample. The transient vibrational spectra were used to identify reaction intermediates and their kinetics, enabling us to determine the detailed dynamics of the photoexcited molecule. TRIR spectra in broad time spanning from 0.3 ps to 1 μs (time order of 10^7) could probe spectral features related to the primary and secondary reactions, providing their kinetics, thereby, the entire photoexcitation dynamics of the target molecule.

Equilibrium IR spectra of **1** had one band at 1843 cm^{-1} due to NO stretching mode. TRIR spectra of 5 mM **1** in DMSO at 293 K were measured in the spectral region of the NO stretching mode (1935 – 1715 cm^{-1}) from 0.3 ps to 1 μs after excitation at 320 nm. As can be seen in fig. S11, TRIR spectra showed a negative band in the position of the NO stretching mode with no transient absorption band, the same as the inverted equilibrium spectrum, suggesting that there is no molecule in the electronically excited state and all the excited molecules undergo photochemical reaction (here, photodissociation of NO). In other words, the NO dissociation quantum yield (QY) is unity. The negative band arises from the depleted population of the reactant due to the photochemical reaction. As the magnitude of the negative band reflects the population of the photodissociated Ru(salophen)(NO)Cl (producing Ru(salophen)Cl radical + NO), the concentration of Ru(salophen)Cl radical (or NO) could be determined from the magnitude. TRIR spectra were measured with two different excitation energy to adjust the initial concentration of the photodissociated Ru(salophen)(NO)Cl (or produced Ru(salophen)Cl radical + NO). Time-dependent concentrations of Ru(salophen)Cl radical (or NO) were determined from the time-dependent amplitudes of the negative band obtained by fitting the TRIR spectra at two different excitation energies (fig. S12). Most (86 ± 2%) of the Ru(salophen)Cl radical (or NO) decreases with a time constant of 15 ± 1 ps and the 15-ps decay does not depend on the initial concentration of the photoproducts. It arises from geminate rebinding of the nascent photoproducts because they are within a solvent cage in this timescale. The remaining photoproduct likely diffused out from the solvent cage and the Ru(salophen)Cl radical may form solvent bound radical, Ru(salophen)(solv)Cl radical. It decreases in the microsecond time scale due to the bimolecular reaction of the radical and NO with a rate constant of $6.3 \pm 0.5 \times 10^9$ $M^{-1}s^{-1}$, which is about twice the calculated diffusion-limited rate constant, implying that the radical is highly reactive with NO and the reaction proceeds in a diffusion-limited rate. Since the radical or NO can react with other compounds (i.e, NO can react with O_2), any measurement of the radical or NO at a later time scale can underestimate the quantity of these photoproducts. Thus, care must be taken for the determination of QY by the quantity of these photoproducts in the later time scale than any side reaction of these photoproducts.

A kinetic scheme (scheme S1) is introduced to describe the photoexcitation dynamics of **1** derived from the femtosecond TRIR spectra at 320 nm. According to the scheme S1, all the excited **1** in DMSO at 320 nm photodissociates NO. In other words, QY of NO dissociation from **1** in DMSO at 293 K is unity at 320-nm excitation. The majority of the nascent photoproducts (86 ± 2%) geminately rebind with a time constant of 15 ± 1 ps, and remainings bimolecularly rebind with a diffusion-limited rate. Thus, any utilization of produced NO should proceed faster than the bimolecular reaction of NO with the Ru radical.

Fig. S11. Representative time-resolved infrared spectra obtained from 0.3 ps to 1 μs after excitation of Ru(salophen)(NO)Cl (**1**) in DMSO at 320 nm. Data (open circles) were well reproduced by the inverted equilibrium spectra (solid lines). The equilibrium spectra were obtained by the fitting measured equilibrium spectrum using an FT-IR spectrometer.

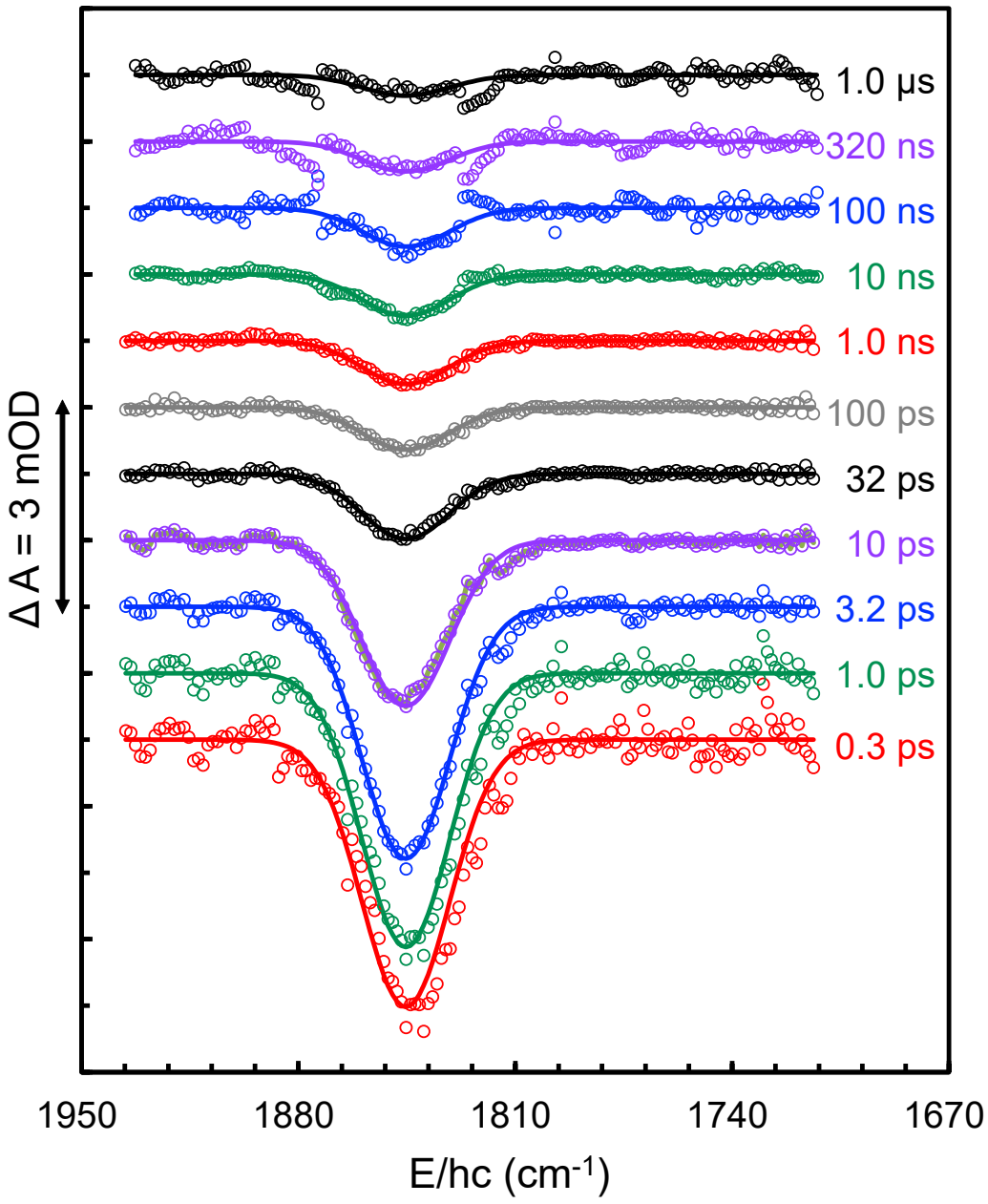

Fig. S12. Time-dependent concentration changes of photoproduct, Ru(salophen)Cl radical or NO, from the excited Ru(salophen)(NO)Cl (**1**) in DMSO at 320 nm at two different excitation energies. The initial concentration was 0.8 (black open circles) or 0.47 (blue open circles) mM. Time-dependent kinetics were well reproduced by the geminate rebinding (GR) with a time constant of 15 ± 1 ps and bimolecular rebinding (BR) of the radical with NO in a diffusion-limited rate constant of $6.3 \pm 0.5 \times 10^9$ $M^{-1}s^{-1}$. Note that the apparent decay rate in high initial concentration is much faster than that in lower initial concentration.

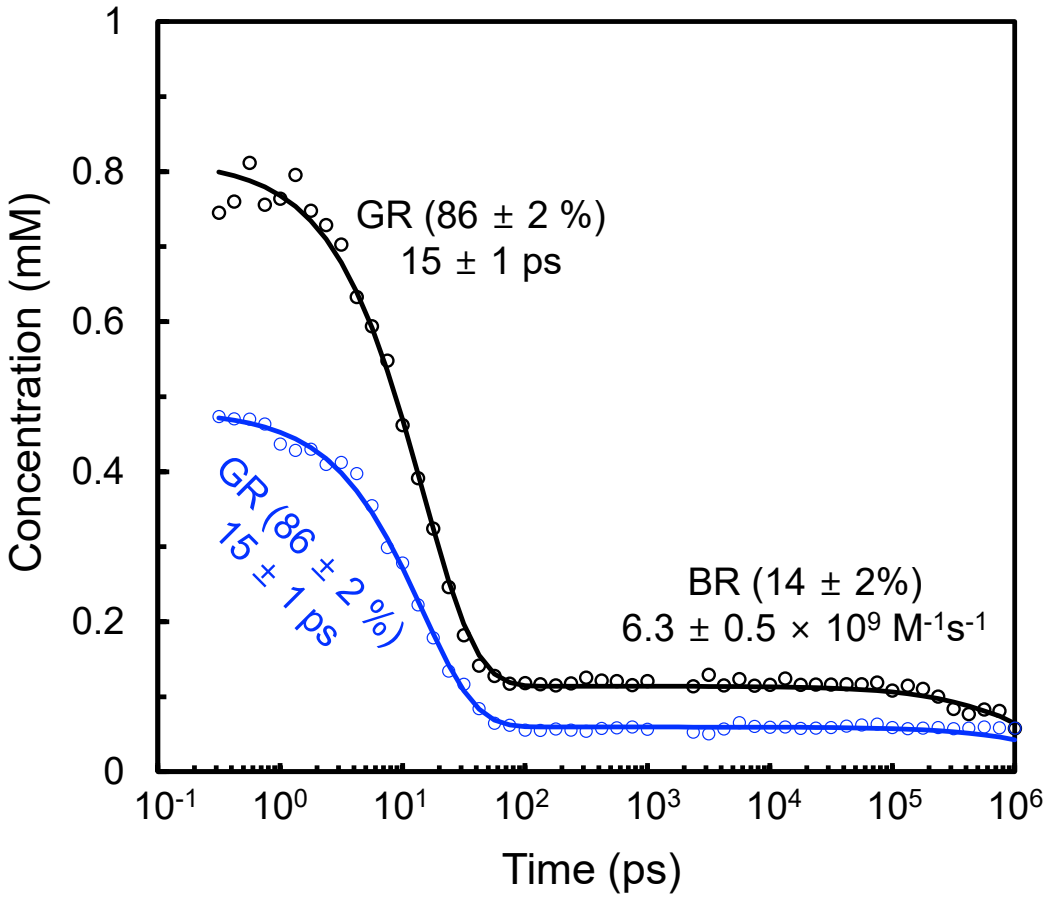

Scheme S1. A kinetic scheme to describe the photoexcitation dynamics of Ru(salophen)(NO)Cl (**RuNO**) in DMSO at 320 nm. All the photoexcited **RuNO** undergoes chemical reaction (CR) producing Ru(salophen)Cl radical (**Ru**) and NO. In other words, there is no non-radiative relaxation (NR) to the lower-lying excited electronic state (**RuNO***), from the photoexcited **RuNO**, that returns to the ground electronic state via electronic relaxation (ER). About 86% of nascent **Ru** undergoes geminate rebinding (GR) with NO and the remaining binds to solvent forming a solvent-bound **Ru** (**Ru-solv**). The **Ru-solv** eventually proceeds with bimolecular rebinding (BR) with NO with a diffusion-limited rate constant.